Energy-based scatter correction and energy dependent image reconstruction for PET scanners

Lucretiu M. Popescu, *Member, IEEE*, Samuel Matej, *Senior Member, IEEE*,
Robert M. Lewitt, *Senior Member, IEEE*, and Joel S. Karp, *Senior Member, IEEE*

***Abstract*— In this paper we propose a comprehensive energy based scatter correction approach for PET. The detailed energy information that comes with the list-mode data, as well as the marked difference between the energy spectra of unscattered and scattered photons are used for the estimation of the scattered events distributions and inside the reconstruction algorithm to individualize the correction terms for each coincidence by taking into account the probability of each event to be a true, a scattered (or a random) given its position and energy information. The central piece of our approach is the two-dimensional detector energy response model represented as a linear combination of four components, each one representing a particular state a PET event can be found in: both photons unscattered, the second scattered while the first not, first photon scattered while the second not, and both photons scattered. For a set of events collected in the vicinity of a given line of response, the coefficient of each component is determined by applying a statistical estimator. As a result we obtain the number of scattered events that are in the given set. The model gives us also the variation of scatter fraction with the photon pair energies for that particular position in the data space.**

I. Introduction

In this paper we propose a comprehensive energy based scatter correction approach for PET, able to take advantage of the new photon detection techniques, which due to better scintillator crystals [1]–[3] and improvements in the associated electronics, allow for more accurate estimation of the energy of the detected particles. The detailed energy information that comes with the list-mode data, as well as the marked difference between the energy spectra of unscattered and scattered photons, are used for the estimation of the scattered events distributions, and inside the reconstruction algorithm, to individualize the correction terms for each event by taking into account the probability of each event to be a true, a scattered (or a random) given its position and energy information.

II. The theoretical model

The central piece of our approach is the two-dimensional detector energy response model represented as a linear combination of four components each one representing a particular state a PET event can be found in

$$C(E_1, E_2) = \sum_{l=0}^{3} \sigma_l e_l(E_1, E_2)\,, \tag{1}$$

The authors are with University of Pennsylvania, Department of Radiology, 423 Guardian Drive, 4-th floor Blockley Hall, Philadelphia, PA 19104-6021, USA, E-mail: popescu@mipg.upenn.edu

This work was supported in part by the National Institutes of Health under Grant No. R33-EB001684.

where E_1, E_2 are the reported energies of the first, respectively second photon of a PET detection event. Here the individual photons in a PET event are distinguished by their position and not by the their detection order. We have σ_0 the number of true coincidences (both photons unscattered), σ_1 the number of events with the second photon scattered while the first not, σ_2 the number of events with the first photon scattered while the second not, and σ_3 the number of events with both photons scattered. Also $e_0(E_1, E_2) = A(E_1)A(E_2)$, $e_1(E_1, E_2) = A(E_1)B(E_2)$, $e_2(E_1, E_2) = B(E_1)A(E_2)$ and $e_3(E_1, E_2) = B(E_1)B(E_2)$, where $A(E)$ is the average detector energy response spectrum of the unscattered photons and $B(E)$ is the average detector energy response spectrum of the scattered photons; A and B are normalized so that $\int_{\mathcal{E}} A(E)\mathrm{d}E = \int_{\mathcal{E}} B(E)\mathrm{d}E = 1$ over the energy range of interest $\mathcal{E}$.

A. Energy based scatter estimation

For a set of events collected in the vicinity of a given line of response (LOR), we can estimate the coefficient of each component by applying a statistical estimator. As a result we obtain the number of scattered events that are in the given set. The model gives us also the variation of scatter fraction with the photons energies for that particular position in the data space.

For performing the fit several methods are available. The simplest is the extension of the dual energy window method for single photons to the case of photon pairs, which in fact is a 2×2 energy window method (two energy windows for each photon). More versatile are the methods that take advantage of each photon individual energy information, such as the moments method or the maximum likelihood method. More details about these methods are given in the appendix.

B. Energy dependent image reconstruction

We denote a point in data space as $\mathbf{y} \equiv (\mathbf{y}^g, \mathbf{y}^e) \in \mathcal{D} \times \mathbb{R}^2$ where $\mathbf{y}^g$ stands for the geometrical coordinates covering the data space $\mathcal{D}$, and $\mathbf{y}^e \equiv (E_1, E_2)$ are the energies of the coincidence detected photon pair. The activity distribution f is discretely represented by $\{f_i\}_{i=\overline{1,I}}$ image elements. The scatter events distribution is modeled using a finite set of coefficients $\sigma \equiv \{\sigma_{1k}, \sigma_{2k}, \sigma_{3k}\}_{k=\overline{1,K}}$ with k indices following the points of a coarse grid that cover uniformly the geometrical data space.

The count rate density in the data point $\mathbf{y}$ for given activity and scattered events distributions is

$$g(\mathbf{y}|f, \sigma) = g_t(\mathbf{y}|f) + g_s(\mathbf{y}|\sigma) \tag{2}$$

where $g_t(\mathbf{y}|f) = e_0(\mathbf{y}^e)\sum_{i=1}^{I} a_i(\mathbf{y}^g) f_i$ is the energy dependent distribution of the true (unscattered) events and $g_s(\mathbf{y}|\sigma) = \sum_{k=1}^{K} b_k(\mathbf{y}^g)\sum_{l=1}^{3} e_l(\mathbf{y}^e)\sigma_{lk}$ is the energy dependent distribution of the scattered photons; $a_i(\mathbf{y}^g)$ is the probability that an emission from voxel i be detected in the data space point $\mathbf{y}^g$, and $b_k(\mathbf{y}^g) = b(\mathbf{y}^g - \mathbf{y}^g_k)$ is an interpolation kernel between scatter grid points.

For a set of N events $Y \equiv \{\mathbf{y}_n\}_{n=\overline{1,N}}$. The likelihood function (the probability density) of Y given f and σ is

$$\mathcal{L}(Y|f,\sigma) = \frac{\Lambda^N}{N!}\mathrm{e}^{-\Lambda}\prod_{n=1}^{N}\frac{1}{\Lambda}g(\mathbf{y}_n|f,\sigma) \tag{3}$$

where Λ is the total (trues and scattered) detection probability, regardless the energies $\Lambda = \int g(\mathbf{y}|f,\sigma)\mathrm{d}\mathbf{y} = \sum_{i=1}^{I} Q_i f_i + \sum_{k=1}^{K}\sum_{l=1}^{3}\sigma_{lk}$ with $Q_i = \int_{\mathcal{D}} a(\mathbf{y}^g)\mathrm{d}\mathbf{y}^g$ is the detection sensitivity for image element i.

The activity distribution f, and that of scattered photons σ, most likely to fit the data can be obtained by using maximum likelihood expectation maximization algorithm (ML-EM) with the following iterative update equations

$$f_i^{(m+1)} = f_i^{(m)}\frac{1}{Q_i}\sum_{n=1}^{N}\frac{a_i(\mathbf{y}_n^g)e_0(\mathbf{y}_n^e)}{g_t(\mathbf{y}_n|f^{(m)}) + g_s(\mathbf{y}_n|\sigma^{(m)})} \tag{4}$$

$$\sigma_{lk}^{(m+1)} = \sigma_{lk}^{(m)}\sum_{n=1}^{N}\frac{b_k(\mathbf{y}_n^g)e_l(\mathbf{y}_n^e)}{g_t(\mathbf{y}_n|f^{(m)}) + g_s(\mathbf{y}_n|\sigma^{(m)})} \tag{5}$$

If equation (4) is used alone with the scatter coefficients $(\sigma_{1k}, \sigma_{2k}, \sigma_{3k})$ estimated prior to the image reconstruction through an external procedure, then we have an ML-EM image reconstruction algorithm with energy dependent scatter correction.

If the equations (5) are used independently and the term $g_t(\mathbf{y}|f)$ is replaced with the zero-th order scatter component $b_k(\mathbf{y}^g)e_0(\mathbf{y}^e)\sigma_{0k}$ we obtain the ML-EM equation for energy based estimation of the scatter components $(\sigma_{0k}, \sigma_{1k}, \sigma_{2k}, \sigma_{3k})$.

III. Simulation Study

We considered a cylindrical PET scanner with 84 cm diameter and 24 cm length. For studying the energy spectra of scattered and unscattered photons we modeled an inhomogeneous phantom with shape similar to that of the Utah phantom. The physical dimensions of the phantom can be seen in Fig. 1, where sections through the attenuation map and activity distribution are shown. The activity distribution follows that of the attenuation coefficient with the values in the two cylindrical cold regions 0.2 times background activity. The phantom's attenuation and activity distributions are extended axially outside the scanner field of view. A large hot sphere with radius 2.5 cm and contrast 4:1 is placed off center in the middle region. In order to reduce further the system symmetry we shifted the phantom 3 cm along the y axis.

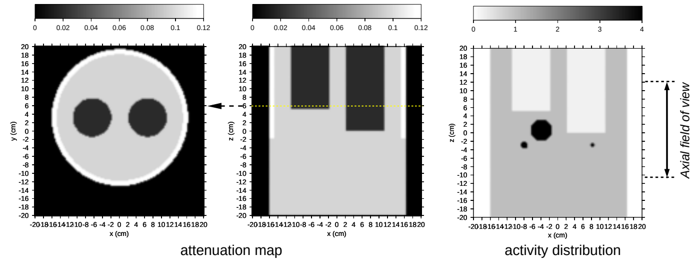

Fig. 1. Sections of the inhomogeneous phantom used. The background is water equivalent, while the two cylindrical cold regions have the attenuation coefficient 20% of that of water.

The data were generated using the Monte Carlo simulation program described in [4]–[6] by considering an analog simulation of the photon transport through the phantom and a simplified model for the photon detection using Gaussian distributions for the the energy and time of flight (TOF) resolutions. Detailed information about each detected photon pair, including the energies, the TOF data, and flags indicating the scattered photons were saved in a list using a compact format described in [7]. In this study we have not considered random coincidences.

Here we present results for two scatter estimation cases performed with the energy based moments method as described in appendix B and using the following four (m, n) pairs of moments $\{(0,0), (1,2), (2,1), (2,2)\}$. First we considered a non-TOF case and modeled an energy resolution $\varepsilon_E = 6.4\%$ relative standard deviation ($\approx$ 15% relative FWHM). Second we considered a TOF case with a positioning precision along LOR of $\sigma_l = 3.0$ cm ($\approx$ 470 ps FWHM timing resolution) and energy resolution $\varepsilon_E = 4.0\%$ ($\approx$ 9% FWHM). The data space is represented using the (ϕ, θ, u, v, l) coordinates where ϕ and θ are the usual polar angles designating a direction in space, u and v are position coordinates in the projection plane and l represents the estimated position along a LOR estimated from TOF data. Further in the text when not specified otherwise the numerical values for angles will be given in degrees and for the lengths in centimeters; directions with $\theta = 90°$ are perpendicular to the scanner axis. The scatter data was calculated for a grid using a spacing of $\Delta\phi$ and $\Delta\theta$ of 5°, Δu and Δv of 2 cm, and in the TOF case $\Delta l = 1.17\sigma_l$. In order to reduce the statistical fluctuations and obtain smoother scatter estimations, the counts were spread among nearby u, v and l bins using weights given by bell shaped kernels $b(x) = \left[1 - (x/R)^2\right]^2$ along each direction with a maximum radius of $R = r \times \Delta$ where Δ is the grid spacing along a given dimension; we used $r \approx 2$ for u, v and l dimensions. In both cases the data lists contained about 15 million true events. We set an energy threshold of 440 keV for the $\varepsilon_E = 6.4\%$ case, and 450 keV for the $\varepsilon_E = 4\%$ case.

In Fig. 2 are shown the energy spectra for non-scattered (A) and scattered photons (B) for several positions in the data space, and the overall average, determined from Monte Carlo data for the non-TOF and 15% FWHM energy resolution case. One can notice that while the low energy tail of the B spectra shape varies significantly with the position, the high energy portion is more stable, hence for a high enough energy threshold

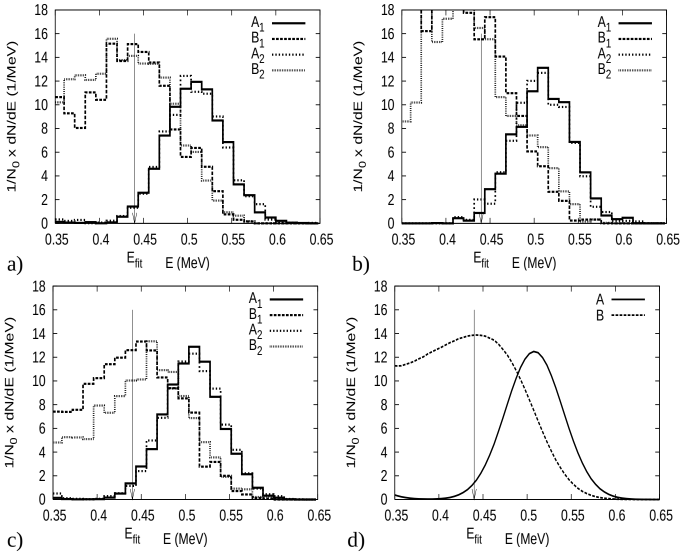

Fig. 2. The energy spectra $A(E)$ for not scattered, and $B(E)$ for scattered PET photons at several positions in the data space as determined from Monte Carlo data for the non-TOF and 15% relative FWHM energy resolution case. The spectra are normalized to unity for $E > E_{\mathrm{fit}}$ region, and correspond to the following (ϕ, θ, u, v) data space points: a) for $(0, 90, 20, 6)$, b) for $(0, 90, -18, 6)$ and c) for $(90, 90, -12, 6)$. In the d) case spectra shown are the averages over all of the data domain used for the scatter estimation.

E_{fit}, a unique B shape will represent a robust approximation.

The plots in Fig. 3 and Fig. 4 show a good agreement with Monte Carlo data. In the TOF case one can notice the significant variation of the scatter with the TOF position and, although we have a better energy resolution, the fit has to overcome the scarcity of counts in each TOF bin.

In order to further test our concept we adapted a recently developed TOF list-mode image reconstruction algorithm in order to accept energy dependent correction terms and coefficients. Aspects of the reconstruction algorithm used here were recently described in [7], [8]. The reconstructed images were represented using blobs — smooth overlapping basis functions [9], [10] — on a face centered cubic grid and we used iterations over subsets made from consecutive events in the list. Further in the text a complete pass through the data will be referred to as an iteration.

We performed a multi-realization study using a cylindrical phantom of 32 cm diameter symmetrically placed along the axis of the scanner. The phantom features were placed in two slices each at 2.5 cm distance from the scanner central slice. In each slice we have considered 10 identical hot spheres uniformly placed on the circle of radius 8 cm. In this arrangement the distance between hot spheres is greater than 5 cm, therefore the correlation between spheres in the same image is small enough to enable us to consider each reconstructed sphere as a independent realization. By this means in each reconstructed volume we will obtain 20 realizations of each type of feature and with a few reconstructed images (3–5) we obtain a statistically significant number of feature realizations.

Four image reconstruction cases were compared. The first

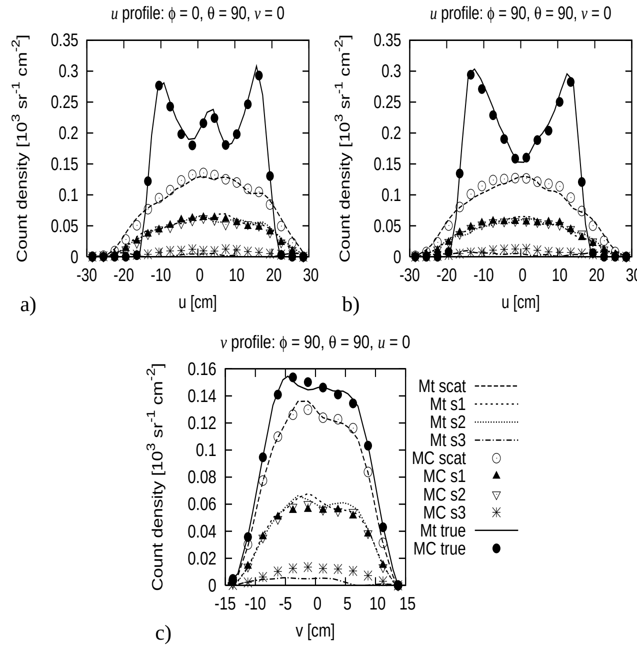

Fig. 3. Comparison between the scatter estimates obtained with the energy based moments method (Mt) and the Monte Carlo data (MC), for a non-TOF case and energy resolution $\varepsilon_E = 6.4\%$ (15% relative FWHM). The cases a) and b) represent two orthogonal projections of the central slice, while c) represents an axial profile. In the legend s_1, s_2 are the partial scatter count densities in the case when the first, respectively the second, PET photon is scattered while the other not, and s_3 corresponds to the case with both photons scattered.

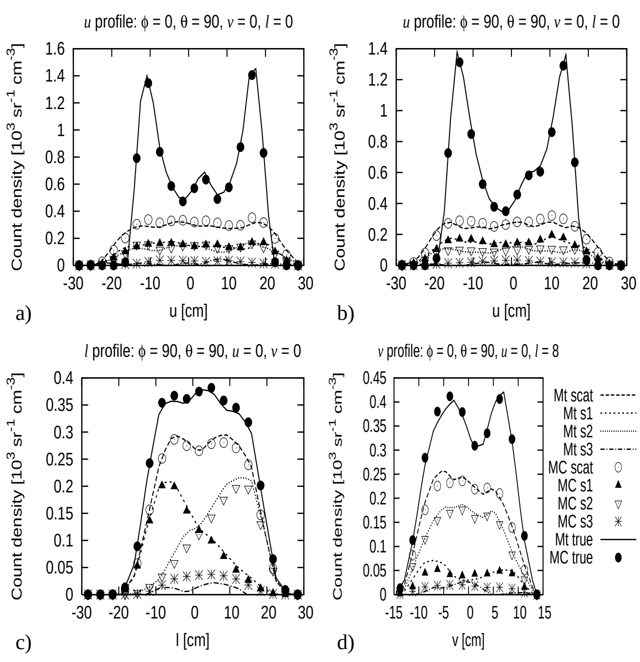

Fig. 4. Comparison between the scatter estimates obtained with the energy based moments method (Mt) and the Monte Carlo data (MC), as in Fig. 3 this time for a TOF case with $\sigma_l = 3.0$ cm ($\approx$ 470 ps FWHM timing resolution) and energy resolution $\varepsilon_E = 4.0\%$ (9.4% relative FWHM). The cases a) and b) represent two orthogonal projections of the central slice and central TOF position, the case c) correspond to a longitudinal profile along a LOR, while the case d) represents an axial profile.

— no scatter correction (sn) — all events with energies above the reconstruction threshold were used and no scatter correction was applied. In the second — scatter removed (sr) — the events marked as scattered were not used. The other two cases we used scatter corrections estimated with the energy based method using ML-EM approach in similar conditions as in the tests presented above, with $E_{\text{fit}} = 450$ keV and $E_{\text{rec}} = 460$ keV. In one case — energy dependent scatter (se) — we used the equation (4) with the prior estimated scatter coefficients $\{\sigma_{lk}\}$. In the last case — static scatter correction (ss) — was used the traditional scatter correction approach by considering only the estimated total scatter distribution in each point $g_s(\mathbf{y}^g) = \sum_{k=1}^{K} b_k(\mathbf{y}^g) \sum_{l=1}^{3} \sigma_{lk}$, applied by eliminating from equation (4) all the $e_l(\mathbf{y}^e)$ factors.

Multiple image realizations were obtained by using distinct data sets containing 12 million true coincidences, with an energy resolution of $\varepsilon_E = 3.4\%$ (8% relative FWHM) for non-TOF and TOF cases with $\sigma_l = 3$ cm ($\approx$ 470 ps FWHM timing resolution). Hot spheres with contrast 4:1 and 0.5 cm radius were considered. For each realization of a sphere of radius R we measured the signal S as the image average inside the sphere and the background B as the image average outside the sphere and within a radius $2R + 0.5$ cm from the center of the sphere. The contrast is defined as $C = \frac{|S-B|}{B}$ and the contrast recovery coefficient is CRC $= \frac{C}{C_0} \times 100$, where C_0 is the original phantom contrast. For each sphere we computed the average CRC over all realizations obtained. The uncertainties of these estimations (as statistical sample standard deviations σ_f) were also computed. For the noise estimation we computed also the standard deviations σ_b of the same spherical regions at similar fixed position but with the signal absent (background only regions). As in the case of non prewhitening matched filter observer (NPWMF) the noise was evaluated as $\sqrt{\frac{1}{2}(\sigma_f^2 + \sigma_b^2)}$.

The contrast as function of iteration number and contrast versus noise plots presented in Fig. 5 show, as expected, that the scatter removed (sr) ideal method systematically performs better than the others, while the no scatter correction (sn) case is relatively largely biased if compared with any other method. The energy dependent correction (se) represents an improvement over the static scatter correction (ss).

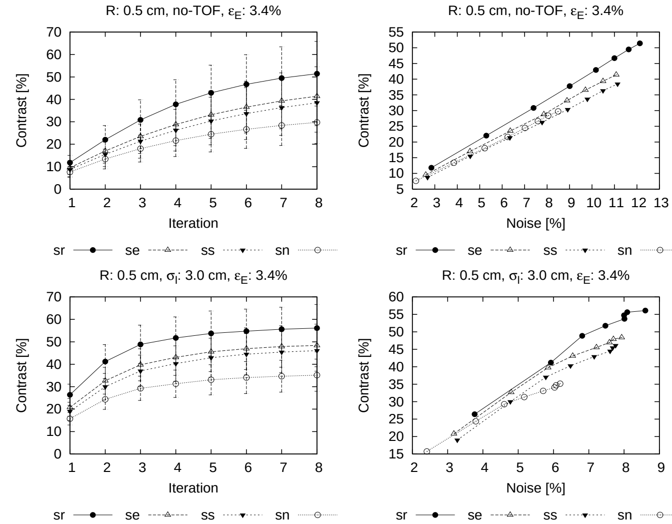

Fig. 5. Comparisons between contrast as function of iteration number and contrast versus noise plots for no scatter correction (sn) case, scatter events removed (sr) case, static scatter correction (ss) case, and the energy dependent scatter correction (se) method. Top plots show a non-TOF case, bottom plots show a TOF case.

IV. Discussions and Conclusions

We can conclude from these numerical experiments that the energy based scatter estimation method is feasible in the cases when the energy resolution is good enough so that the photopeak shape A does not spread over the less stable portion of the shape B. Also, the improved results produced by the energy dependent reconstruction method compared with the simple — not energy dependent — scatter correction approach illustrate the importance the accurate modeling of the physical effects plays in the quality of the images obtained.

The difference between the energy based scatter estimation part of our approach and the previous dual energy window (DEW) type approaches applied in PET [11]–[14], consists mainly in the four energy component model we are proposing, that leads to the estimation of four independent coefficients. The previous DEW methods in PET attempted to empirically estimate the scatter fraction by establishing a proportionality relation of some sort between the number of counts collected in the energy windows used, overlooking the fact that, when symmetries are broken, the total scatter fraction in reality is the sum of at least three independent parameters. When used with the moments method or the maximum likelihood method our approach benefits also from the more detailed energy information that comes with list-mode data. Compared with the image reconstruction methods that use energy dependent weights [15], our energy-based image reconstruction approach uses scatter corrections that vary both with the LOR position and energy, while in the aforementioned methods the variation with the LOR position is neglected.

Compared with the current most widely used image based method for scatter correction [16]–[20] our energy based approach inherently considers the scatter from outside the field of view, it estimates the scatter distribution in absolute values eliminating the need for the error prone tail fitting scaling, and the method provides directly the position and energy dependent scatter corrections necessary for the energy-dependent image reconstruction. The single scatter simulation method can be modified in order to provide two of the components (single scatter fractions for each photon in a PET pair). With the third (double scatter fraction) neglected or empirically estimated from the first two, one can still use the model we propose to perform an energy dependent image reconstruction. However, if we take into consideration the revival of interest in the time of flight PET and the continuous bed movement design option pondered by the scanner manufacturers nowadays, then the image based scatter estimation methods would be required to produce simulation results that accurately cover a considerably larger multidimensional space, a fact that will be at least inconvenient if not computationally too expensive. The energy based method estimates the scatter distribution as a function of position and energies by only performing a simple statistical analysis of the population of events recorded, and therefore it is considerably more convenient and flexible.

Appendix

A. The 2×2 energy window method

The extension of the dual energy window method to the case of photon pairs gives us a 2×2 energy window method (two energy windows for each photon). Let N_0 be the observed number of photon pairs with both energies in the window $\mathcal{E}_0$, N_1 the number of events with $(E_1, E_2) \in \mathcal{E}_0 \times \mathcal{E}_1$, N_2 the number of events with $(E_1, E_2) \in \mathcal{E}_1 \times \mathcal{E}_0$ and N_3 the number of events with $(E_1, E_2) \in \mathcal{E}_1 \times \mathcal{E}_1$. Matching the observed data with the energy model predictions we obtain the following system of linear equations that can be easily solved

$$\left\{ \begin{array}{rcl} \sigma_0\alpha_0^2 + \sigma_1\alpha_0\beta_0 + \sigma_2\beta_0\alpha_0 + \sigma_3\beta_0^2 & = & N_0 \\ \sigma_0\alpha_0\alpha_1 + \sigma_1\alpha_0\beta_1 + \sigma_2\beta_0\alpha_1 + \sigma_3\beta_0\beta_1 & = & N_1 \\ \sigma_0\alpha_1\alpha_0 + \sigma_1\alpha_1\beta_0 + \sigma_2\beta_1\alpha_0 + \sigma_3\beta_1\beta_0 & = & N_2 \\ \sigma_0\alpha_1^2 + \sigma_1\alpha_1\beta_1 + \sigma_2\beta_1\alpha_1 + \sigma_3\beta_1^2 & = & N_3 \end{array} \right. , \quad (6)$$

where $\alpha_0 = \int_{\mathcal{E}_0} A(E)\mathrm{d}E$, $\alpha_1 = \int_{\mathcal{E}_1} A(E)\mathrm{d}E$, $\beta_0 = \int_{\mathcal{E}_0} B(E)\mathrm{d}E$, $\beta_1 = \int_{\mathcal{E}_1} B(E)\mathrm{d}E$.

B. The moments method

We can estimate the moment of order (m, n) of the energy distribution of the photon pairs by computing the quantity $\hat{q}_{mn} = \sum_{i=1}^{N} E_{1,i}^m E_{2,i}^n$, which should match the theoretical value

$$\begin{aligned} q_{mn} &= \iint E_1^m E_2^n C(E_1, E_2)\mathrm{d}E_1\mathrm{d}E_2 \\ &= \sigma_0 a_m a_n + \sigma_1 a_m b_n + \sigma_2 b_m a_n + \sigma_3 b_m b_n , \quad (7) \end{aligned}$$

with $a_m = \int_{\mathcal{E}} E^m A(E)\mathrm{d}E$, $b_n = \int_{\mathcal{E}} E^n B(E)\mathrm{d}E$

By conveniently selecting four combinations (m, n) we can obtain an equation system as in the case of dual energy window method (6).

C. The ML-EM method

Using notations similar to those used in section II-B, for a given region in the data space the expected number of counts is $\Lambda = \sum_{l=0}^{3} \sigma_l$. The energy distribution is $\frac{1}{\Lambda}\sum_{l=0}^{3} \sigma_l e_l(\mathbf{y}^e)$. For a data set $Y_E \equiv \{\mathbf{y}_1^e, \ldots, \mathbf{y}_N^e\}$ the likelihood function is

$$\mathcal{L}(Y_E|\sigma) = \frac{\Lambda^N}{N!}\mathrm{e}^{-\Lambda} \prod_{n=1}^{N} \frac{1}{\Lambda} \sum_{l=0}^{3} \sigma_l e_l(\mathbf{y}_n^e) \quad (8)$$

Maximum likelihood corresponds to the point for which $\frac{\partial \ln \mathcal{L}(Y_E|\sigma)}{\partial \sigma_l} = 0$, and can be reached using the following ML-EM iterative update equation

$$\sigma_l^{(m+1)} = \sigma_l^{(m)} \sum_{n=1}^{N} \frac{e_l(\mathbf{y}_n^e)}{\sum_{k=0}^{3} \sigma_k^{(m)} e_k(\mathbf{y}_n^e)} , \quad l = 0, 1, 2, 3 \quad (9)$$

References

[1] C. W. E. van Eijk, P. Dorenbos, E. V. D. van Loef, K. W. Krämer, and H. U. Güdel, “Energy resolution of some new inorganic-scintillator gamma-ray detectors,” *Radiation Measurements*, vol. 33, pp. 521–525, 2001.

[2] E. V. D. van Loef, P. Dorenbos, C. W. E. van Eijk, K. W. Krämer, and H. U. Güdel, “Scintillation properties of $LaBr_3$:Ce^{3+} crystals: fast, efficient and high-energy-resolution scintillator,” *Nucl. Instr. Meth. Phys. Res. A*, vol. 484, pp. 254–258, 2002.

[3] W. W. Moses, “Current trends in scintillator detectors and materials,” *Nucl. Instr. Meth. Phys. Res. A*, vol. 487, pp. 123–128, 2002.

[4] L. M. Popescu and R. M. Lewitt, “A versatile approach for Monte Carlo simulation of tomographic systems,” in *IEEE Nucl. Sci. Symp. Conf. Rec.*, vol. 4, pp. 2785 – 2788, 19-25 Oct. 2003.

[5] L. M. Popescu, “A computer code package for Monte Carlo electron-photon transport simulation. Comparisons with experimental benchmarks,” *Nucl. Instr. Meth. Phys. Res. B*, vol. 161-163, pp. 318–322, 2000.

[6] L. M. Popescu, “A geometry modelling system for ray tracing or particle transport Monte Carlo simulation,” *Comp. Phys. Comm.*, vol. 150, no. 1, pp. 21–30, 2003.

[7] L. M. Popescu, S. Matej, and R. M. Lewitt, “Iterative image reconstruction using geometrically ordered subsets with list-mode data,” in *IEEE Nucl. Sci. Symp. Conf. Rec.*, vol. 6, pp. 3536 – 3540, 16-22 Oct. 2004.

[8] L. M. Popescu and R. M. Lewitt, “Ray tracing through a grid of blobs,” in *IEEE Nucl. Sci. Symp. Conf. Rec.*, vol. 6, pp. 3983 – 3986, 16-22 Oct 2004.

[9] R. M. Lewitt, “Alternatives to voxels for image representation in iterative reconstruction algorithms,” *Phys. Med. Biol.*, vol. 37, no. 3, pp. 705–716, 1992.

[10] S. Matej and R. M. Lewitt, “Efficient 3D grids for image reconstruction using spherically-symmetric volume elements,” *IEEE Trans. Nucl. Sci.*, vol. 42, no. 4, pp. 1361–1370, 1995.

[11] B. Bendriem, R. Trebossen, V. Frouin, and A. Syorta, “A PET scatter correction using simultaneous acquisition with low and high lower energy thresholds,” in *IEEE Med. Img. Conf. Rec.*, (San Francisco), pp. 1779–1783, 1993.

[12] S. Grootoonk, T. J. Spinks, D. Sashin, N. M. Spyrou, and T. Jones, “Correction for scatter in 3D PET using dual energy window method,” *Phys. Med. Biol.*, vol. 41, pp. 2757–2774, 1996.

[13] L. Shao, R. Freifelder, and J. S. Karp, “Triple energy window scatter correction technique in PET,” *IEEE Trans. Med. Imag.*, vol. 13, no. 4, pp. 641–648, 1994.

[14] L.-E. Adam, J. S. Karp, and R. Freifelder, “Energy-based scatter correction for 3-D PET scanner using NaI(Tl) detectors,” *IEEE Trans. Med. Imag.*, vol. 19, no. 5, pp. 513–521, 2000.

[15] H.-T. Chen, C.-M. Kao, and C.-T. Chen, “A fast, energy-dependent scatter reduction method for 3D PET imaging,” in *IEEE Nucl. Sci. Symp. Conf. Rec.*, vol. 4, pp. 2630–2634, 19-25 Oct 2003.

[16] J. M. Ollinger, “Model-based scatter correction for fully 3D PET,” *Phys. Med. Biol.*, vol. 41, pp. 153–176, 1996.

[17] C. C. Watson, D. Newport, and M. E. Casey, “A single scatter simulation technique for scatter correction in 3D PET,” in *Three-Dimensional Image Radiation and Nuclear Medicine* (P. Grangeat and J.-L. Amans, eds.), pp. 255–268, Kluwer, 1996.

[18] C. C. Watson, “New, faster, image-based scatter correction for 3D PET,” *IEEE Trans. Nucl. Sci.*, vol. 47, no. 4, pp. 1587–1594, 2000.

[19] A. Werling, O. Bublitz, J. Doll, L.-E. Adam, and G. Brix, “Fast implementation of the single scatter simulation algorithm and its use in iterative image reconstruction of PET data,” *Phys. Med. Biol.*, vol. 47, pp. 2947–2960, 2002.

[20] R. Accorsi, L.-E. Adam, M. E. Werner, and J. S. Karp, “Optimization of a fully 3D single scatter simulation algorithm for 3D PET,” *Phys. Med. Biol.*, vol. 49, no. 12, pp. 2577–2598, 2004.